Ultrathin PEGylated $W_{18}O_{49}$ Nanowires as a New 980 nm-Laser-Driven Photothermal Agent for Efficient Ablation of Cancer Cells In Vivo

Zhigang Chen, Qian Wang, Huanli Wang, Lisha Zhang, Guosheng Song, Linlin Song, Junqing Hu,* Hongzhi Wang, Jianshe Liu, Meifang Zhu,* and Dongyuan Zhao*

Dedicated to Professor Chun-Hui Huang on the occasion of her 80th birthday

Near-infrared (NIR) laser-induced photothermal ablation (PTA) therapy has attracted increasing interest as a minimally invasive and potentially more effective treatment alternative to conventional approaches such as surgery, radiation therapy, and chemotherapy for cancer treatment.[1–18] To promote the photothermal conversion efficiency and, in particular, to improve the lasers' discrimination, a prerequisite for the development of NIR laser-induced PTA is to obtain biocompatible and efficient photothermal coupling agents. Currently, four types of photothermal agents have been extensively developed, resulting in great contributions to progress in PTA therapy.[1–18] The first type are organic compounds such as indocyanine green (ICG) dye[1] and polyaniline nanoparticles,[2] but they may suffer from limitations such as photobleaching and/or unsatisfactory photothermal conversion efficiency. The second type are carbon-based materials, including carbon nanotubes (CNTs)[3] and graphene,[4] which have relatively low absorption coefficient in the NIR region. The third type are metal nanostructures, including Ge nanoparticles,[5] Pd-based nanosheets,[6] and Au nanostructures (supramolecularly assembled nanoparticles,[7] nanorods,[8] nanoshells,[9] hollow nanospheres,[10] nanocages,[11] nanocrosses,[12] and nanostars[13]). These noble metal–based nanostructures exhibit intense NIR photoabsorption and are the most studied photothermal agents, but they are very expensive, which will limit their widespread application. The last type are copper chalcogenide semiconductors, including CuS[14] and $Cu_{2-x}Se$[15] nanoparticles, and Au/CuS nanocomposites.[16] We have also prepared CuS superstructures[17] and Cu_9S_5 nanoparticles[18] as 980 nm laser-driven photothermal agents. The main limitation of copper chalcogenides is their unsatisfactory photothermal conversion efficiency. To meet the severe requirements of future PTA therapy, it is still necessary to develop novel kinds of photothermal agents.

It has been revealed that besides noble metal materials, transition metal oxides are also interesting candidates with localized surface plasmon resonances (LSPRs).[19] Among them, tungsten oxide (WO_{3-x}) nanocrystals are of great interest because of strong LSPRs, which give rise to strong photoabsorption in the NIR region.[19b] In particular, very recently monoclinic $W_{18}O_{49}$ has attracted considerable attention in various applications, such as transparent smart windows[20] and photocatalysts,[21] owing to its unusual defect structure and intense NIR photoabsorption. These features also trigger our interest in the novel concept of developing $W_{18}O_{49}$ as a new kind of transition metal oxide–based photothermal agent. In this Communication, we report the preparation of ultrathin PEGylated $W_{18}O_{49}$ nanowires — where PEG is poly(ethylene glycol) — by a simple solvothermal route. These nanowires exhibit strong NIR photoabsorption and can be used as a 980 nm-laser-driven photothermal agent for the efficient PTA of in vivo cancer cells.

In the work presented here, ultrathin PEGylated $W_{18}O_{49}$ nanowires were prepared by solvothermally treating an ethanol and PEG (molecular weight MW = 400 Da, abbreviated as PEG-400) mixture solution containing WCl_6 at 180 °C for 24 h. The solvent composition has an obvious effect on the size of the $W_{18}O_{49}$ nanowires. When only ethanol was used as the solvent, the $W_{18}O_{49}$ sample consisted of bundle-like nanowires with lengths of up to several micrometers (Figure S1 in the Supporting Information), and these bundle-like nanowires were in fact composed of a lot of individual nanowires with thickness of about 0.9 nm, which is similar to a previous result.[21] It should be noted that these $W_{18}O_{49}$ nanowires are too long for biological application. To shorten the length of the $W_{18}O_{49}$ nanowires and to increase their surface chemical groups and biocompatibility,

Prof. Z. G. Chen, G. S. Song, L. L. Song, Prof. J. Q. Hu, Prof. H. Z. Wang, Prof. M. F. Zhu
State Key Laboratory for Modification of Chemical Fibers and Polymer Materials
College of Materials Science and Engineering
Donghua University, Shanghai 201620, P. R. of China
E-mail: zgchen@dhu.edu.cn; hu.junqing@dhu.edu.cn; zmf@dhu.edu.cn

Dr. Q. Wang
Department of Orthopedics
Shanghai First People's Hospital Affiliated to Shanghai Jiaotong University
Shanghai 200080, P. R. of China

H. L. Wang, Dr. L. S. Zhang, Prof. J. S. Liu
College of Environmental Science and Engineering
Donghua University
Shanghai 201620, P. R. of China

Prof. Z. G. Chen, Prof. D. Y. Zhao
Laboratory of Advanced Materials
Department of Chemistry
Fudan University,
Shanghai 200433, P. R. of China

DOI: 10.1002/adma.201204616

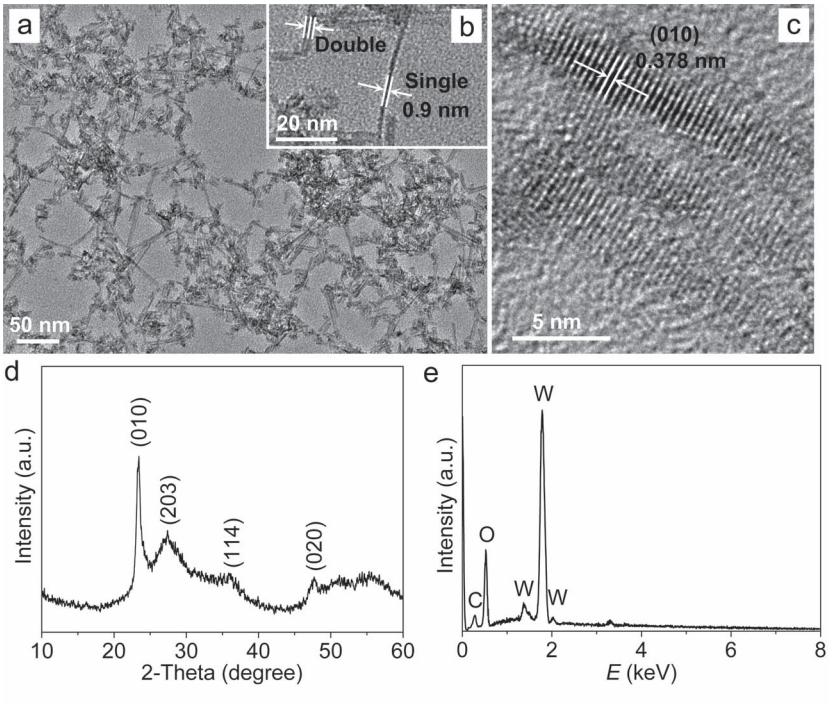

Figure 1. TEM (a,b) and HRTEM (c) images, and XRD (d) and EDS (e) patterns of $W_{18}O_{49}$ nanowires.

PEG-400 was added to ethanol solution as a co-solvent and ligands. When the mixture solvent consisted of 40 vol% PEG-400, the nanowires had a length of 80–400 nm (Figure S2 in the Supporting Information). Interestingly, if the volume ratio of PEG-400 to ethanol was increased to 7/3, the average lengths of the nanowires dropped to about 50 nm, as demonstrated in the transmission electron microscopy (TEM) images (Figure S2B in the Supporting Information and **Figures 1**a–c). Obviously, the presence of a high concentration of PEG-400 can prevent the stacking of the nanowire unit, resulting in the formation of some single nanowires and/or double-nanowire stacks (Figure 1b). These nanowires have a thickness of about 0.9 nm and width of about 4 nm. Furthermore, the high-resolution TEM (HRTEM) image (Figure 1c) also indicates clear lattice fringes, suggesting that the nanowire is a single crystal. The interplanar *d*-spacing, determined to be 0.378 nm, agrees with the (010) lattice fringes of monoclinic phase $W_{18}O_{49}$, suggesting that the nanowire grows along the [010] direction, which is similar to the previous reports.[20–22] In addition, Figure 1d shows the X-ray diffraction (XRD) pattern, and all peaks could be well indexed to the monoclinic $W_{18}O_{49}$ phase (JCPDS no. 71-2450). The narrow (010) and (020) peaks also indicate that the crystal growth direction of $W_{18}O_{49}$ nanowires should be [010], since the close-packed planes of monoclinic-phase $W_{18}O_{49}$ crystal are {010},[21] which agrees well with the above HRTEM image (Figure 1c). Energy-dispersive X-ray spectroscopy (EDS) further confirmed that there were only W and O elements in the $W_{18}O_{49}$ nanowire sample (Figure 1e).

Surface functional chemical groups of the $W_{18}O_{49}$ nanowires are important for their biological application. The presence of PEG-400 ligands on the surface of $W_{18}O_{49}$ nanowires can be confirmed by the Fourier transform infrared spectrum (Figure S3 in the Supporting Information). As a result, PEGylated $W_{18}O_{49}$ nanowires are hydrophilic and can be readily dispersed in water and in some polar organic solvents, such as dimethylformamide (DMF) or dimethyl sulfoxide (DMSO). The aqueous dispersion containing 2 mg mL^{-1} $W_{18}O_{49}$ nanowires exhibited a strong blue color (the inset of **Figure 2**), and had high stability, even remaining unchanged for a week. The optical property of the aqueous dispersion was studied using UV-vis-NIR spectroscopy (Figure 2). The spectrum is similar to what has been reported previously for $W_{18}O_{49}$ nanowires,[21] and it exhibits a short-wavelength absorption edge at approximately 420 nm, which agrees well with the reported value for the bandgap (E_g = 2.9 eV), and reaches a minimum at around 510 nm. Importantly, $W_{18}O_{49}$ nanowires exhibit enhanced photoabsorption as the wavelength increases from 510 to 1100 nm. Several theories have been proposed[19b,20] for the origin of NIR photoabsorption of tungsten oxides (WO_{3-x}), the most widely accepted models being LSPRs,[19b] intervalence charge transfer,[23] and small polaron absorption.[24] In fact, in all these three accepted models, NIR photoabsorption can be considered to be closely related to the free electrons and/or oxygen-deficiency-induced small polarons.

The strong NIR photoabsorption of PEGylated $W_{18}O_{49}$ nanowires motivated us to investigate their potential in PTA therapy of cancer with a 980 nm wavelength laser. Under irradiation with the 980 nm laser with a power density of 0.72 W cm^{-2}, which is safe for human skin exposure,[25] the temperature elevation of aqueous dispersions containing $W_{18}O_{49}$ nanowires at different concentrations (0–3 g L^{-1}) was measured (**Figure 3**). The blank test demonstrates that the temperature of

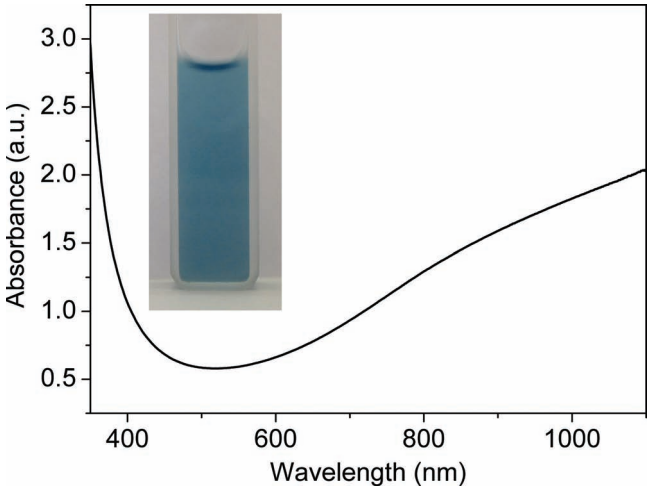

Figure 2. UV-vis absorption spectrum of an aqueous dispersion containing 2 g L^{-1} $W_{18}O_{49}$ nanowires. Inset: Photo of the aqueous dispersion.

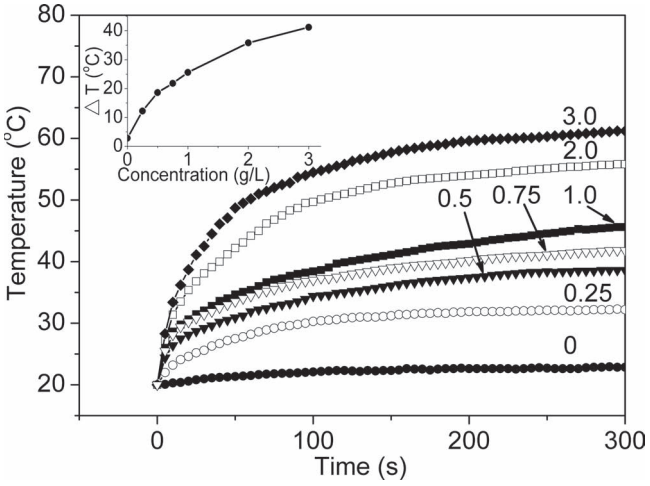

Figure 3. Temperature elevation of aqueous dispersions of $W_{18}O_{49}$ nanowires with different concentrations (0–3.0 g L^{-1}) as a function of time (0–300 s) under irradiation with a 980 nm-wavelength laser at a safe power density (0.72 W cm^{-2}). Inset: Temperature change (ΔT) over a period of 300 s versus $W_{18}O_{49}$ concentration.

pure water (without $W_{18}O_{49}$ nanowires) increased by less than 3 °C from the room temperature of 20 °C. With the addition of $W_{18}O_{49}$ nanowires (0.25–3.0 g L^{-1}), the temperature of the aqueous dispersion increased by 12.2–41.2 °C in 5 min; the heating rate became slower with a further increase of temperature owing to faster heat loss at higher temperature.[17] Thus, one can conclude that $W_{18}O_{49}$ nanowires can rapidly and efficiently convert the 980 nm-wavelength laser energy into heat energy, which results from strong photoabsorption at 980 nm. In addition, the temperature change (ΔT) in 300 s, which is calculated from Figure 3, goes up dramatically with an increase of $W_{18}O_{49}$ nanowire concentration from 0 to 2 g L^{-1}, and then flattens out upon further increase of $W_{18}O_{49}$ nanowire concentration to 3 g L^{-1} (the inset in Figure 3). This phenomenon can be attributed to fast heat loss at relatively high temperature and is similar to our previous reports on CuS superstructures[17] and Cu_9S_5 nanoparticles.[18]

The ideal photothermal coupling agents should be nontoxic for biological applications. To evaluate the cytotoxicity of PEGylated $W_{18}O_{49}$ nanowires, an MTT [3-(4,5-dimethylthiazol-2-yl)-2,5-diphenyltetrazolium bromide] assay with the human cervical carcinoma cell line HeLa was used to determine their effects on cell proliferation after 24 h. No significant differences in the cell proliferation were observed in the absence or presence of 0.25–3.0 g L^{-1} $W_{18}O_{49}$ nanowires (Figure S4 in the Supporting Information). The cellular viability was estimated to be greater than 90% after 24 h. These data show that the aqueous dispersion of PEGylated $W_{18}O_{49}$ nanowires (<3 g L^{-1}) can be considered to have low cytotoxicity.

As is well known, hyperthermic therapy is the use of heat between 40 and 45 °C to damage cancer cells.[17,26] If it is assumed that the temperature of the in vivo human body is 36 °C, human tumor tissues, after being injected with an aqueous dispersion of $W_{18}O_{49}$ nanowires and even if covered by 0–1 mm thick skin, can easily be heated to over 45 °C in 5 min by irradiation with a 980 nm-wavelength laser with a safe power density of 0.72 W cm^{-2}, probably resulting in the efficient death of cancer cells. In the study presented here, the biomedical application of PEGylated $W_{18}O_{49}$ nanowires as photothermal agents was evaluated by PTA of cancer cells in mice. Severe combined immunodeficiency (SCID) mice were inoculated subcutaneously with 2×10^6 K7M2 cells for 21 days. When the tumors inside the mice had grown to 5–10 mm in diameter, the SCID mice were randomly allocated into treatment and control groups. The SCID mice in the treatment group were injected with 100 μL of $W_{18}O_{49}$ nanowire phosphate-buffered saline (PBS) solution (2g L^{-1}) at the central region of the tumor with a depth of ca. 4 mm, while the SCID mice in the control group were injected with 100 μL saline solution. After 1 h, mice from both the control and treatment groups were simultaneously irradiated by two similar 980 nm-wavelength laser devices at 0.72 W cm^{-2} power density for 10 min. During the laser treatment, full-body thermographic images were captured using an IR camera (inset in **Figure 4**a, Figure S5 and video in the Supporting Information). The temperature of the irradiated area was recorded as a function of the irradiation time (Figure 4a). For the mice injected with saline solution, the surface temperature of the tumor increased by less than 1.5 °C, and remained below 27.5 °C during the entire irradiation process, indicating a negligible temperature elevation. Importantly, in the case of $W_{18}O_{49}$ nanowire–injected mice, the tumor surface temperature increased rapidly to reach 44.5 °C at 30 s and 49.1 °C at 60 s, and then began to plateau at 50.0 ± 0.5 °C after 120 s, as demonstrated vividly in Figure S5 and the video (Supporting Information). A typical thermographic image at 180 s is shown in the inset of Figure 4a. These facts reveal a rapid elevation of temperature of the in vivo tumor, suggesting that $W_{18}O_{49}$ nanowires within the tumor still have an excellent photothermal effect, because of the deep penetration depth of 980 nm-wavelength laser light in biological tissues as demonstrated in our previous reports.[25]

Subsequently, the in vivo tumors were removed, embedded in paraffin, and cryosectioned into 4 μm slices. The slides were stained with hematoxylin/eosin (H&E). The histological examination of tumors was performed by means of microscopic imaging (Figures 4b,c and Figure S6 in the Supporting Information). In the case of saline-injected mice, there are no obvious differences regarding the cells' size and shape, nuclear modifications, or necrosis after the irradiation with the 980 nm-wavelength laser (Figure 4b). This suggests that the low heat energy converted from the 980 nm-wavelength laser by saline solution and/or tissues, which is related to the negligible elevation (<1.5 °C) of the tumor temperature, is not enough to kill the cancer cells. On the other hand, in the case of $W_{18}O_{49}$ nanowire–injected mice, the common signs of thermal cell necrosis are presented on most areas of the examined tumor slide in the entire tumor mass (Figure S6 in the Supporting Information and Figure 4c). Furthermore, one can find more detailed changes of the cancer cells, such as shrinkage of the malignant cells, loss of contact, eosinophilic cytoplasm, and nuclear damage (pyknotic and fragmentized nuclei). Besides the destruction of the tumor cells, thermal injury was also observed in the stromal reactive tissue, for example, the connective tissue surrounding the tumor cells was disrupted with fragmented collagen fibers (Figure S6, Supporting Information).

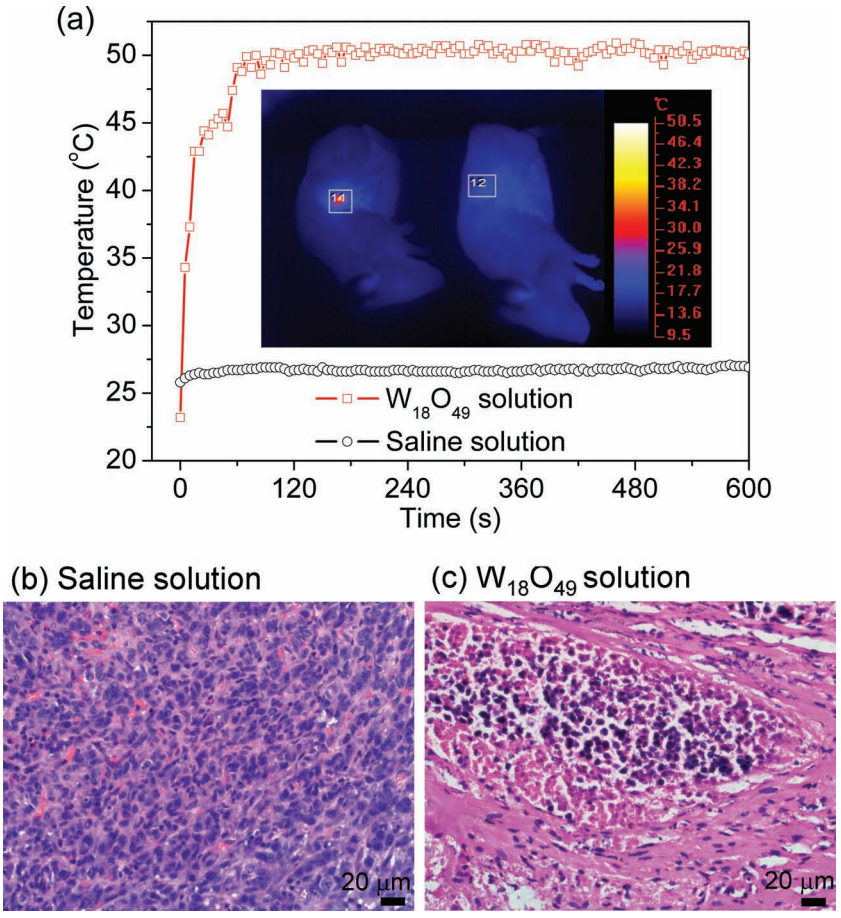

Figure 4. a) Plots of the temperature within the irradiated tumor area in two mice injected respectively with saline solution and $W_{18}O_{49}$ nanowire PBS solution (2 g L^{-1}), as a function of irradiation time. The inset is the corresponding full-body thermographic image of mice respectively injected with saline solution (right mouse) and $W_{18}O_{49}$ nanowire PBS solution (left mouse) at 180 s. b,c) H&E-stained histological images of the corresponding ex vivo tumor sections, after irradiation for 10 min. The irradiation source is a 980 nm laser with the safe power density of 0.72 W cm^{-2}.

These facts suggest that in vivo cancer cells can be efficiently destroyed by the high temperature (ca. 50 °C) arising from the excellent photothermal effect of PEGylated $W_{18}O_{49}$ nanowires. Therefore, PEGylated $W_{18}O_{49}$ nanowires have great potential to be used as a novel and excellent photothermal agent for PTA of specific targets such as in vivo tumor tissues. To the best of our knowledge, this is the first time that PTA of cancer cells in vivo has been realized using a transition metal oxide nanocrystal itself as the photothermal agent under irradiation with a 980 nm-wavelength laser. For future commercial use of PTA therapy technology, further research should be done, for example, by conjugating target biomolecules on the surface of PEGylated $W_{18}O_{49}$ nanowires, and/or optimizing the wavelength of the NIR laser to below or above 980 nm because of the presence of the absorption band of water at 980 nm.

In summary, ultrathin PEGylated $W_{18}O_{49}$ nanowires have been prepared by a simple solvothermal route with a mixture of ethanol and poly(ethylene glycol) (PEG-400) as the solvent. The aqueous dispersion of $W_{18}O_{49}$ nanowires exhibits a strong blue color, and has enhanced absorption with an increase of wavelength in the NIR region. Under irradiation with a 980 nm-wavelength laser with a safe power density of 0.72 W cm^{-2}, the temperature of the nanowire aqueous dispersion (0.25–3.0 g L^{-1}) can increase by 12.2–41.2 °C in 5 min. Importantly, the temperature of an in vivo tumor injected with $W_{18}O_{49}$ nanowire solution (100 μL, 2 g L^{-1}) increased rapidly to 50.0 ± 0.5 °C after 120 s irradiation, resulting in the efficient PTA of cancer cells in 10 min. Therefore, these PEGylated $W_{18}O_{49}$ nanowires demonstrate great superiority as a new photothermal agent for NIR-induced PTA of cancer, as a result of their small size and high photothermal conversion efficiency as well as their low cost and low cytotoxicity. More importantly, this work provides some insight into the research and development of other transition metal oxide nanocrystals as novel photothermal agents for PTA therapy.

Experimental Section

Synthesis of ultrathin PEGylated $W_{18}O_{49}$ nanowires: PEGylated $W_{18}O_{49}$ nanowires were prepared by a modified solvothermal route.[21] In a typical procedure, WCl_6 (0.4 g) was dissolved in a mixture (100 mL) of poly(ethylene glycol) (molecular weight MW = 400 Da, abbreviated as PEG-400) and ethanol with a volume ratio of 7/3. Then the solution was magnetically stirred, forming a transparent yellow solution. Subsequently, the resulting solution was transferred to a poly(tetrafluoroethylene) (Teflon)-lined stainless steel autoclave, sealed, and treated at 180 °C for 24 h. A blue precipitate was collected by centrifugation and washed with ethanol several times. Finally, the precipitate was dried in vacuum at 50 °C for 24 h. For comparison, pure ethanol or a mixture of PEG-400 and ethanol with a volume ratio of 4/6 were also used as the solvent to prepare $W_{18}O_{49}$ nanowires.

Characterization and measurement of photothermal performance: The size, morphology, and microstructure of $W_{18}O_{49}$ nanowires were determined by HRTEM (JEOL JEM-2010F). XRD measurements were performed on a Bruker D4 X-ray diffractometer using Cu Kα radiation (λ = 0.15418 nm). EDS of the sample was carried out on a Bruker Quantax 400 EDS system attached to a Hitachi S-4800 field emission scanning electron microscope. The Fourier transform infrared (FTIR) spectrum was measured from samples in KBr pellets using an IRPrestige-21 spectrometer (Shimadzu). UV-vis absorption spectra were measured on a Shimadzu UV-2550 UV–visible–NIR spectrophotometer using quartz cuvettes with an optical path of 1 cm.

To measure the photothermal conversion performances of ultrathin PEGylated $W_{18}O_{49}$ nanowires, radiation from a 980 nm laser was sent through a quartz cuvette containing an aqueous dispersion (0.3 mL) of $W_{18}O_{49}$ nanowires with different concentrations (0–3 g L^{-1}); the light source was an 980 nm-wavelength semiconductor laser device (Xi'an Tours Radium Hirsh Laser Technology Co., Ltd., P. R. of China) whose power could be adjusted externally (0–0.3 W). The output power was independently calibrated using a hand-held optical power meter (Newport model 1918-C, CA, USA) and was found to be ca. 0.29 W for a spot size of ca. 0.40 cm^2 (ca. 0.72 W cm^{-2}). A thermocouple with an accuracy of ±0.1 °C was inserted into the aqueous dispersion perpendicular to the path of the laser. The temperature was measured every 5 s.

Cytotoxicity Assay and PTA of Cancer Cells In Vivo: The in vitro cytotoxicity was measured using the methyl thiazolyl tetrazolium (MTT)

assay in the human cervical carcinoma cell line HeLa, which is similar to our previous report.[18] Cells growing in a log phase were seeded into a 96-well cell culture plate at 5×10^4 per well in DMEM (Dulbecco's modified Eagle's medium, which contains 10% fetal bovine serum, 4 mM glutamine, 100 U mL^{-1} penicillin, 100 mg mL^{-1} streptomycin, and 1% HEPES (hydroxyethyl piperazine ethanesulfonic acid)) at 37 °C and in the presence of 5% CO_2 for 24 h. Then the cells were incubated with ultrathin PEGylated $W_{18}O_{49}$ nanowires at different concentrations (i.e., 0, 0.25, 0.5, 0.75, 1, 2, and 3 g L^{-1}, diluted in DMEM) at 37 °C for 24 h in the presence of 5% CO_2. Subsequently, 10 μL of MTT (5 mg mL^{-1}) was added to each well of the 96-well assay plate and incubated for a further 4 h at 37 °C in the presence of 5% CO_2. After the addition of 10% sodium dodecyl sulfate (SDS, 100 mL/well), the assay plate was allowed to stand at room temperature for 12 h. A Thermo Scientific Multiskan MK3 monochromator-based multifunction microplate reader was used to measure the absorbance of each well with background subtraction at 492 nm. All of the tests were independently performed three times.

The PTA of cancer cells in vivo was carried out by a modified method, as described elsewhere.[17,18] Severe combined immunodeficiency (SCID) mice were inoculated subcutaneously with 2×10^6 K7M2 cells in the side of the rear for 21 days. When tumors inside the mice had grown to 5–10mm in diameter, the SCID mice were randomly allocated to two groups (control and treatment groups). The SCID mice in the treatment group were injected with 100 μL PBS solution containing $W_{18}O_{49}$ nanowires (2 g L^{-1}) at the central region of the tumor with a depth of ca. 4 mm, while the SCID mice in the control group were injected with 100 μL saline solution. After 1 h, the mice with tumors from both the control and the treatment groups were simultaneously irradiated by two similar 980 nm laser devices at 0.72 W cm^{-2} for 10 min. During the irradiation with the 980 nm-wavelength laser, full-body thermographic images and temperature were recorded in real time using a photothermal medical device (GX-300; Shanghai Infratest Electronics Co., Ltd, P. R. of China.) with an infrared camera. After the laser treatment, the SCID mice were killed, and tumors were removed, embedded in paraffin, and cryosectioned into 4 μm slices. The slides were stained with H&E. The slices were examined under a Zeiss Axiovert 40 CFL inverted fluorescence microscope, and images were captured with a Zeiss AxioCam MRc5 digital camera.

Supporting Information

Supporting Information is available from the Wiley Online Library or from the author.

Acknowledgements

This work was financially supported by the National Natural Science Foundation of China (Grant nos. 21107013, 21171035, 50902021, 50925312, and 51272299), the High-Tech Research and Development Program of China (2012AA030309), the Key Grant Project of the Chinese Ministry of Education (Grant no. 313015), the Specialized Research Fund for the Doctoral Program of Higher Education (20110075120012), the Scientific Research Foundation for Returned Overseas Chinese Scholars, the Shanghai Rising-Star Program (Grant no. 11QA1400100), the Science and Technology Commission of Shanghai-based "Innovation Action Plan" Project (Grant No. 10JC1400100), the Innovation Program of Shanghai Municipal Education Commission (Grant no. 13ZZ053), the Shanghai Leading Academic Discipline Project (Grant no. B603), and the Fundamental Research Fund for the Central Universities.

Received: November 7, 2012
Revised: December 30, 2012
Published online: February 21, 2013

[1] J. Yu, D. Javier, M. A. Yaseen, N. Nitin, R. Richards-Kortum, B. Anvari, M. S. Wong, *J. Am. Chem. Soc.* **2010**, *132*, 1929.
[2] J. Yang, J. Choi, D. Bang, E. Kim, E. K. Lim, H. Park, J. S. Suh, K. Lee, K. H. Yoo, E. K. Kim, Y. M. Huh, S. Haam, *Angew. Chem. Int. Ed.* **2011**, *50*, 441.
[3] a) J. W. Kim, E. I. Galanzha, E. V. Shashkov, H. M. Moon, V. P. Zharov, *Nat. Nanotechnol.* **2009**, *4*, 688; b) H. K. Moon, S. H. Lee, H. C. Choi, *ACS Nano* **2009**, *3*, 3707; c) X. Wang, C. Wang, L. Cheng, S.-T. Lee, Z. Liu, *J. Am. Chem. Soc.* **2012**, *134*, 7414.
[4] a) K. Yang, S. Zhang, G. X. Zhang, X. M. Sun, S. T. Lee, Z. Liu, *Nano Lett.* **2010**, *10*, 3318; b) J. T. Robinson, S. M. Tabakman, Y. Y. Liang, H. L. Wang, H. S. Casalongue, D. Vinh, H. J. Dai, *J. Am. Chem. Soc.* **2011**, *133*, 6825; c) Z. M. Markovic, L. M. Harhaji-Trajkovic, B. M. Todorovic-Markovic, D. P. Kepic, K. M. Arsikin, S. P. Jovanovic, A. C. Pantovic, M. D. Dramicanin, V. S. Trajkovic, *Biomaterials* **2011**, *32*, 1121; d) K. Yang, L. Hu, X. Ma, S. Ye, L. Cheng, X. Shi, C. Li, Y. Li, Z. Liu, *Adv. Mater.* **2012**, *24*, 1868; e) M. Li, X. Yang, J. Ren, K. Qu, X. Qu, *Adv. Mater.* **2012**, *24*, 1722; f) S.-H. Hu, Y.-W. Chen, W.-T. Hung, I. W. Chen, S.-Y. Chen, *Adv. Mater.* **2012**, *24*, 1748.
[5] T. N. Lambert, N. L. Andrews, H. Gerung, T. J. Boyle, J. M. Oliver, B. S. Wilson, S. M. Han, *Small* **2007**, *3*, 691.
[6] X. Huang, S. Tang, B. Liu, B. Ren, N. Zheng, *Adv. Mater.* **2011**, *23*, 3420.
[7] a) J. Nam, N. Won, H. Jin, H. Chung, S. Kim, *J. Am. Chem. Soc.* **2009**, *131*, 13639; b) S. T. Wang, K. J. Chen, T. H. Wu, H. Wang, W. Y. Lin, M. Ohashi, P. Y. Chiou, H. R. Tseng, *Angew. Chem. Int. Ed.* **2010**, *49*, 3777; c) A. Buchkremer, M. J. Linn, M. Reismann, T. Eckert, K. G. Witten, W. Richtering, G. von Plessen, U. Simon, *Small* **2011**, *7*, 1397.
[8] a) X. H. Huang, I. H. El-Sayed, W. Qian, M. A. El-Sayed, *J. Am. Chem. Soc.* **2006**, *128*, 2115; b) J. L. Li, D. Day, M. Gu, *Adv. Mater.* **2008**, *20*, 3866; c) G. von Maltzahn, A. Centrone, J. H. Park, R. Ramanathan, M. J. Sailor, T. A. Hatton, S. N. Bhatia, *Adv. Mater.* **2009**, *21*, 3175; d) C. Ungureanu, R. Kroes, W. Petersen, T. A. M. Groothuis, F. Ungureanu, H. Janssen, F. W. B. van Leeuwen, R. P. H. Kooyman, S. Manohar, T. G. van Leeuwen, *Nano Lett.* **2011**, *11*, 1887; e) J. Wang, G. Zhu, M. You, E. Song, M. I. Shukoor, K. Zhang, M. B. Altman, Y. Chen, Z. Zhu, C. Z. Huang, W. Tan, *ACS Nano* **2012**, *6*, 5070.
[9] a) J. Yang, J. Lee, J. Kang, S. J. Oh, H. J. Ko, J. H. Son, K. Lee, J. S. Suh, Y. M. Huh, S. Haam, *Adv. Mater.* **2009**, *21*, 4339; b) H. T. Ke, J. R. Wang, Z. F. Dai, Y. S. Jin, E. Z. Qu, Z. W. Xing, C. X. Guo, X. L. Yue, J. B. Liu, *Angew. Chem. Int. Ed.* **2011**, *50*, 3017.
[10] a) J. You, G. D. Zhang, C. Li, *ACS Nano* **2010**, *4*, 1033; b) S. Preciado-Flores, D. C. Wang, D. A. Wheeler, R. Newhouse, J. K. Hensel, A. Schwartzberg, L. H. Wang, J. J. Zhu, M. Barboza-Flores, J. Z. Zhang, *J. Mater. Chem.* **2011**, *21*, 2344.
[11] a) J. Y. Chen, D. L. Wang, J. F. Xi, L. Au, A. Siekkinen, A. Warsen, Z. Y. Li, H. Zhang, Y. N. Xia, X. D. Li, *Nano Lett.* **2007**, *7*, 1318; b) M. S. Yavuz, Y. Cheng, J. Chen, C. M. Cobley, Q. Zhang, M. Rycenga, J. Xie, C. Kim, K. H. Song, A. G. Schwartz, L. V. Wang, Y. Xia, *Nat. Mater.* **2009**, *8*, 935; c) J. Y. Chen, C. Glaus, R. Laforest, Q. Zhang, M. X. Yang, M. Gidding, M. J. Welch, Y. N. Xia, *Small* **2010**, *6*, 811.
[12] E. Y. Ye, K. Y. Win, H. R. Tan, M. Lin, C. P. Teng, A. Mlayah, M. Y. Han, *J. Am. Chem. Soc.* **2011**, *133*, 8506.
[13] H. Yuan, A. M. Fales, T. Vo-Dinh, *J. Am. Chem. Soc.* **2012**, *134*, 11358.
[14] a) Y. B. Li, W. Lu, Q. A. Huang, M. A. Huang, C. Li, W. Chen, *Nanomedicine* **2010**, *5*, 1161; b) M. Zhou, R. Zhang, M. A. Huang, W. Lu, S. L. Song, M. P. Melancon, M. Tian, D. Liang, C. Li, *J. Am. Chem. Soc.* **2010**, *132*, 15351.
[15] C. M. Hessel, V. P. Pattani, M. Rasch, M. G. Panthani, B. Koo, J. W. Tunnell, B. A. Korgel, *Nano Lett.* **2011**, *11*, 2560.
[16] S. B. Lakshmanan, X. Zou, M. Hossu, L. Ma, C. Yang, W. Chen, *J. Biomed. Nanotechnol.* **2012**, *8*, 883.
[17] Q. W. Tian, M. H. Tang, Y. G. Sun, R. J. Zou, Z. G. Chen, M. F. Zhu, S. P. Yang, J. L. Wang, J. H. Wang, J. Q. Hu, *Adv. Mater.* **2011**, *23*, 3542.

[18] Q. W. Tian, F. R. Jiang, R. J. Zou, Q. Liu, Z. G. Chen, M. F. Zhu, S. P. Yang, J. L. Wang, J. H. Wang, J. Q. Hu, *ACS Nano* **2011**, *5*, 9761.
[19] a) J. B. Goodenough, *Prog. Solid State Chem.* **1971**, *5*, 145; b) K. Manthiram, A. P. Alivisatos, *J. Am. Chem. Soc.* **2012**, *134*, 3995.
[20] C. Guo, S. Yin, M. Yan, M. Kobayashi, M. Kakihana, T. Sato, *Inorg. Chem.* **2012**, *51*, 4763.
[21] G. Xi, S. Ouyang, P. Li, J. Ye, Q. Ma, N. Su, H. Bai, C. Wang, *Angew. Chem. Int. Ed.* **2012**, *51*, 2395.
[22] J. Polleux, N. Pinna, M. Antonietti, M. Niederberger, *J. Am. Chem. Soc.* **2005**, *127*, 15595.
[23] B. W. Faughnan, R. S. Crandall, P. M. Heyman, *RCA Rev.* **1975**, *36*, 177.
[24] O. F. Schirmer, V. Wittwer, G. Baur, G. Brandt, *J. Electrochem. Soc.* **1977**, *124*, 749.
[25] a) Z. G. Chen, L. S. Zhang, Y. G. Sun, J. Q. Hu, D. Y. Wang, *Adv. Funct. Mater.* **2009**, *19*, 3815; b) L. S. Zhang, Q. W. Tian, W. J. Xu, X. Y. Kuang, J. Q. Hu, M. F. Zhu, J. S. Liu, Z. G. Chen, *J. Mater. Chem.* **2012**, *22*, 18156.
[26] J. van der Zee, *Ann. Oncol.* **2002**, *13*, 1173.